

Chapter 40

A Novel Approach for Biaxial Residual Stress Mapping Using the Contour and Slitting Methods

Mitchell D. Olson and Michael R. Hill

Abstract This paper describes a residual stress measurement approach that determines a two-dimensional map of biaxial residual stress. The biaxial measurement is a combination of contour method, slitting method measurements on a thin slices removed adjacent to the contour plane, and a computation to account for the effects of slice removal. The measurement approach uses only mechanical stress release methods, which is advantageous for some measurement articles. The measurement approach is verified with independent confirmation measurements. Biaxial mapping measurements are performed in a long aluminum bar (77.8 mm width, 51.2 mm thickness, and 304.8 mm length) that has residual stresses induced with quenching. The measured stresses are consistent with quench induced residual stress, having peak magnitude of 150 MPa and a distribution that is tensile toward the center of the bar and compressive around the boundary. The validating confirmation measurement results have good agreement with results from the biaxial mapping approach.

Keywords Residual stress measurement • Contour method • Slitting • Validation • Quenching

40.1 Introduction

Residual stress can play a role in many failure mechanisms. Fatigue [1, 2] and stress corrosion cracking [3–6] are particularly sensitive to the presence of tensile residual stresses. Residual stresses can be difficult to predict because they are often the result of complex manufacturing processes, which makes their measurement important for both understanding failure [7, 8] and for validation of computational models of stress inducing processes [9–14].

Many methods exist for measuring residual stress, and each provides a limited portion of the stress tensor and has various limitations. For example, large samples or samples with difficult microstructure (e.g., texture, large grains, etc.) are difficult to measure with diffraction techniques [15]. Conversely, some mechanical stress relief methods are prone to systematic errors for large magnitude residual stresses [16], especially if the stresses concentrate during sectioning [17, 18]. One mechanical stress relief method, the contour method, has been found to be especially useful since it inherently measures a map of residual stress over a cross-section. The contour method measures the *change* in stress when cutting a part in half (at the cut plane). Since the cut has created a free surface, the stress normal to the cut plane must be zero after the cut, so that the contour method completely determines the out-of-plane stress component that existed at the cut plane, prior to cutting. Pagliaro et al. [19] further showed that the contour method also determines the change in stress for the in-plane normal components of residual stress at the cut plane. Therefore, additional measurements of in-plane stresses on the cut surface can be used to determine the original in-plane stresses. The first measurement of this type was performed in [19] and used X-ray diffraction and hole drilling to measure the remaining in-plane stress at the contour cut plane (after the contour measurement). Our recent work has extended this methodology to use only mechanical stress release methods [20, 21], but that extension requires validation.

This paper describes an approach for mechanical biaxial residual stress mapping. The approach is then carried out on a quenched bar, and the residual stresses determined are validated with complementary measurements.

M.D. Olson (✉) • M.R. Hill
Department of Mechanical and Aerospace Engineering, University of California, One Shields Avenue,
Davis, CA 95616, USA
e-mail: molson@ucdavis.edu

40.2 Methods

40.2.1 Measurement Approach

The new measurement approach comprises multiple mechanical stress release measurements, in conjunction with stress analysis and superposition, to determine multiple stress components at a single plane of interest in a body. Each mechanical stress release measurement will change the part configuration (i.e., change the geometry of the part) and each configuration will be denoted with a capital letter (e.g., A, B, C). The residual stress tensor in each configuration, at the plane of interest, is indicated with a superscripted σ (e.g., σ^A). The biaxial stress mapping approach determines the out-of-plane stress, σ_{zz} , and one component of the in-plane stress, either σ_{xx} or σ_{yy} , at the plane of interest; by obvious extension, a triaxial mapping approach could be applied, if three stress components were needed.

The configuration changes comprising the new approach are shown in Fig. 40.1a and include cutting the part in half at the plane of interest (configuration A to B) and removing a thin slice (configuration B to C) adjacent to the plane of interest. The coordinates assumed in work are shown in Fig. 40.1, with x and y lying in the plane of interest, and z along the length. Using superposition, the stress in configuration A can be found with

$$\sigma^A(x, y, 0) = \sigma^i(x, y, 0) + \sigma^B(x, y, 0) = \sigma^i(x, y, 0) + \sigma^{ii}(x, y, 0) + \sigma^C(x, y, 0) \quad (40.1)$$

where σ with a superscripted Roman numeral denotes the stress released by a change of configuration, defined as the stress in the current configuration subtracted from the stress in the prior configuration (e.g., $\sigma^i = \sigma^A - \sigma^B$). Although (40.1) applies at all spatial locations, our concern is only the plane of interest, at $z=0$. The contour method is used to determine σ^i , and this measurement completely determines the out of plane component (σ_{zz}) of σ^A , since the plane of interest is a free surface in configuration B. The slitting method is used to determine one in-plane component of σ^C .

As shown in Fig. 40.1b, σ^A can be decomposed so that

$$\sigma^A(x, y, 0) = \sigma^{A(z)}(x, y, 0) + \sigma^C(x, y, 0) \quad (40.2)$$

where $\sigma^{A(z)}$ is the effect of the out-of-plane stress on the thin slice of configuration C, which can be determined using σ_{zz} found by the contour method. Furthermore, $\sigma^{A(z)}$ is a theoretical construct that gives the change in stress that would occur in a thin slice, if the out-of-plane stress were removed; and it is the sum of σ^i and σ^{ii} . Using (40.1) and (40.2), only σ^i and σ^C need to be measured to find σ^A , thus there is no need to directly measure σ^{ii} . A locally smooth stress field is required so that $\sigma^C(x, y, 0)$ can be assumed equal to an average of $\sigma^C(x, y, z)$ through the slice thickness. Experimental details are discussed below.

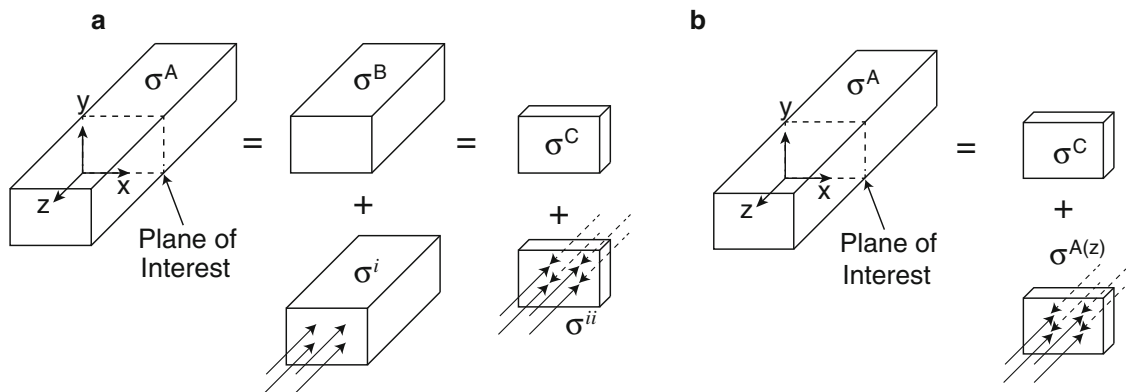


Fig. 40.1 Stress decomposition diagrams. (a) The original stresses (σ^A , all stress components, at the plane of interest) are equal to the stress release from cutting the part in half (σ^i), the stress released when removing a thin slice (σ^{ii}), and the stress remaining in the slice (σ^C). (b) The original stress (σ^A) is equal to the stress remaining in a thin slice (σ^C) plus the effect of total longitudinal stress on the thin slice ($\sigma^{A(z)}$)

40.2.2 Biaxial Mapping

The experimental validation requires two sets of measurements: the first set comprises the biaxial mapping approach itself, and the second set provides additional data that confirm the results from biaxial mapping. Measurements were performed on an aluminum bar that was cut from 51.2 mm (2.02 in.) thick, rolled 7050 aluminum plate to form a 305 mm (12 in.) long bar with a cross section 51.2 mm (2.02 in.) thick by 77.8 mm (3.06 in.) wide, as shown in Fig. 40.2. The original bar was in the T7451 condition, being over-aged and stress relieved by stretching. The bar had an additional heat treatment performed to introduce a higher stress, representative of the T74 temper [22]. The heat treatment consisted of solution heat treatment at 477 °C for 3 h, immersion quenching in room temperature water with 16 % polyalkylene glycol (Aqua-Quench 260), and a dual artificial age at 121 °C for 8 h then 177 °C for 8 h.

The biaxial mapping approach consists of a measurement of σ_{zz} with the contour method [23], removing three thin slices, each 5 mm thick, adjacent to contour measurement cutting plane, and measuring σ_{xx} in the slices with the slitting method [24].

The theoretical underpinning of the contour method has been established earlier by Prime [25] and detailed experimental steps have been established by Prime and DeWald [23]; a brief summary of the experimental procedure is given here, which followed the practical advice in [23]. The specimen is cut in two using a wire electric discharge machine (EDM) along the plane of interest, at the mid-length of the bar (Fig. 40.2). Cutting is performed with the specimen rigidly clamped to the EDM frame. Following cutting, the profile of each of the two opposing cut faces is measured with a laser scanning profilometer to determine the surface height normal to the cut plane as a function of in-plane position. The surface height data are taken on a grid of points with spacing of 200 μm 200 μm , so that there are roughly 96,000 data points for each surface. The two surface profiles are then averaged on a common grid, and the average is fit to a smooth bivariate Fourier series [26], where the number of coefficients in the surface is determined by the choice of the maximum fitting parameters (m, n) for the (x, y) spatial dimensions. A level of smoothing is determined by choosing the fitting parameters (m, n) during data reduction.

The residual stress on the contour plane is found with a linear elastic finite element analysis that applies the negative of the smoothed surface profile as a displacement boundary condition on the cut plane. The finite element mesh used eight-node, linear displacement brick elements with node spacing of 1 mm on the cut face, and node spacing normal to the cut face that increased with distance away from the cut, being 1 mm at the cut face and 5 mm at the end of the bar. The mesh was

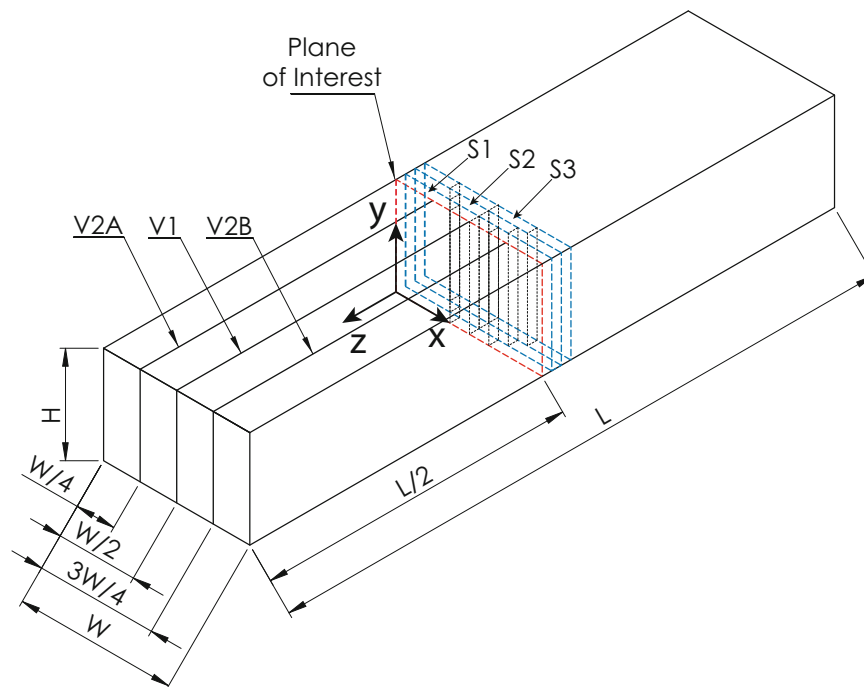


Fig. 40.2 Dimensioned diagram of the measurement article with the location of measurement planes ($W = 77.8$ mm, $H = 51.2$ mm, and $L = 304.8$ mm). The biaxial measurement plane is at $z = 0$ mm and the three confirmation measurements ($V1$, $V2A$ and $V2B$) are at $x = 38.9$, 19.45 , and 58.35 mm. Three slices were removed adjacent to the plane of interest by cutting at $z = -5$ mm ($S1$), -10 mm ($S2$), and -15 mm ($S3$). Each slice has a slitting measurement at the mid-width of the slice and at ± 10 mm ($S1$), ± 15 mm ($S2$), and ± 20 mm ($S3$) from the mid-width

sufficiently refined such that when the node spacing is halved there is negligible change of stress. The model used an elastic modulus of 71.0 GPa and a Poisson's ratio of 0.33.

To find σ_{xx} in the three removed slices, the slitting method (also known as crack compliance) was used. The theoretical underpinning of the slitting measurements has been given by Prime [27] and best experimental practices have been given by Hill [24]. Slitting measurements consist of incrementally cutting through the sample (along y) using a wire EDM while measuring strain at the back face of the cut plane for each cut increment. The stress normal to the cut plane is then determined from measured strain versus cut depth data using an elastic inverse, with smoothing of the stress profile provided by Tikhonov regularization [28]. The elastic inverse uses a compliance matrix that relates the strain that would be caused by an assumed set of basis functions for each cut depth (for further details, see [29]). The compliance matrix is determined using a plane strain finite element model of the part geometry and a stiffness correction scheme developed by Aydiner and Prime [30] to accurately reflect the finite thickness of the slice.

Since the goal of this work is to determine a map of the stress, multiple slitting measurements are needed, at a set of x positions, and these were made in a set of three slices. The three 5 mm thick slices were removed adjacent to the contour measurement plane by cutting with wire EDM at $z = -5, -10,$ and -15 mm. The slitting measurements provided $\sigma_{xx}(y)$ and were made at x locations symmetric about the mid-width, $x_m = 38.9$ mm. Measurement locations in the first slice were at x_m and at $x_m \pm 10$ mm; measurement locations in the second slice were at x_m and at $x_m \pm 15$ mm; and, measurement locations in the third slice were at x_m and at $x_m \pm 20$ mm.

We assume that the stress near the plane of interest is invariant of z , so that the stresses determined in different slices can be collapsed onto a single measurement plane. Since we are performing multiple slitting measurements on each slice, the effect of previous slitting measurements on the current measurement is needed and is found with a supplemental stress analysis. A detailed description of the supplemental stress analysis is given in [31] and consists of applying the measured stress from a previous slitting measurement as a traction boundary condition at the prior measurement plane, in a finite element model of the part, and extracting the resulting stress at the current measurement site. The total stress, at a given plane is a superposition of the stress measured from slitting and the effect of any prior measurement, determined with a supplemental stress analysis.

To find $\sigma^{A(z)}$, the longitudinal stress field found with the contour method is applied as a traction boundary condition to both in-plane (x - y) faces of a finite element model of the thin slice used in the slitting measurements. The finite element mesh used eight-node, linear interpolation brick elements with node spacing of 1 mm on the cut face, and five elements through the thickness. The material behavior was elastic, using the properties stated earlier.

40.2.3 Confirmation Measurements

Confirmation measurements are required to validate the biaxial mapping approach. To do so, σ_{xx} is measured at specific planes using the contour method on configuration B, the half-length bar. Three contour measurements are made at planes V1, V2A, and V2B shown in Fig. 40.2. The first validation measurement, at plane V1, is made at $x = 38.9$ mm and the second and third measurements are made at $x = 19.45$ mm (plane V2A) and 58.35 mm (plane V2B). The first validation measurement aligns with measurements from the biaxial map, but the second and third measurements are not exactly aligned with the measurement locations from the biaxial map (i.e., slitting measurements were offset in x by 0.55 mm). The transverse stress from the biaxial mapping result will be interpolated from nearby data to evaluate stresses at the same positions. Since the stress in the bar was induced with quenching, it is expected that the stress should be constant along the length of the bar, except near the ends.

The confirmation measurements followed the methods for contour measurement described above. The effect of the measurement at plane V1 on stress at planes V2A and V2B was accounted for using superposition. However, it should be noted that the effect of the contour measurement in the biaxial map at $z = 0$ has not been accounted for in the validation measurements, since its effect roughly one thickness away from $z = 0$ will be negligible. The confirmation contour measurements are cut along the z direction, and determine $\sigma_{xx}(y, z)$ at a set of points with approximately 1 mm in-plane spacing. Since the stress is due to quenching, it is expected to be invariant with z , except near the ends of the half-length bar (at $z = -152$ and 0 mm) where σ_{xx} would be affected by the free surface condition. To compare the results of the confirmation contour measurements with results from the biaxial mapping, we report $\sigma_{xx}(y)$ as an average of results at the set of z -positions farther than one thickness from the free end of the half-length bar (i.e., for $-100 \text{ mm} \leq z \leq -52 \text{ mm}$), rather than reporting results for an arbitrarily chosen value of z . At a given value of y , the uncertainty of the confirmation measurement is taken to be the standard deviation of the values from which the average was determined; at nearly all locations, this uncertainty exceeded underlying uncertainty in the contour measurement.

40.3 Results

40.3.1 Biaxial Mapping

The raw surface profiles from the contour measurement at $z=0$ can be seen in Fig. 40.3. The surface profiles from each side of the cut show similar distributions, which indicate good clamping during cutting. The fitting parameters for the contour measurement selected during data processing are $(m, n)=(1, 1)$. The average and fit surface profiles have shapes similar to the measured surface profiles. Line plots of the surface profile data (Fig. 40.4) show that the fit surface appropriately represents the underlying data.

The longitudinal stress and uncertainty can be seen in Fig. 40.5. The stress has a paraboloid distribution with compressive stresses along the exterior (minimum of -153 MPa) and tensile stresses toward the center (maximum of 157 MPa), as would be expected in a quenched bar [32].

The measured strain for the slitting measurement at $x=18.9$ mm ($x=x_m-20$ mm) is shown in Fig. 40.6a, and the calculated stress is shown in Fig. 40.6b. The stress profile is roughly parabolic, as would be expected from a rapid quench. The strain data and stress results at other planes resemble those at $x=18.9$ mm.

The transverse stress from the biaxial map can be seen in Fig. 40.7. The stresses remaining in the slice, σ^C , are compressive along the exterior (minimum of -90 MPa) and tensile toward the center (maximum of 55 MPa). The effect of the longitudinal stress, $\sigma^{A(z)}$, has a paraboloid distribution, compressive along the exterior (minimum of -70 MPa) and tensile toward the center (maximum of 33 MPa). The total transverse stress also has a paraboloid distribution, being compressive along the exterior (minimum of -160 MPa) and tensile toward the center (maximum of 90 MPa), which is expected for quenched samples. Line plots of the two contributions to the total transverse stress at a horizontal position of 38.9 mm ($x=x_m$) can be seen in Fig. 40.8. The plot shows that both contributions, σ^C and $\sigma^{A(z)}$, are significant parts of the total.

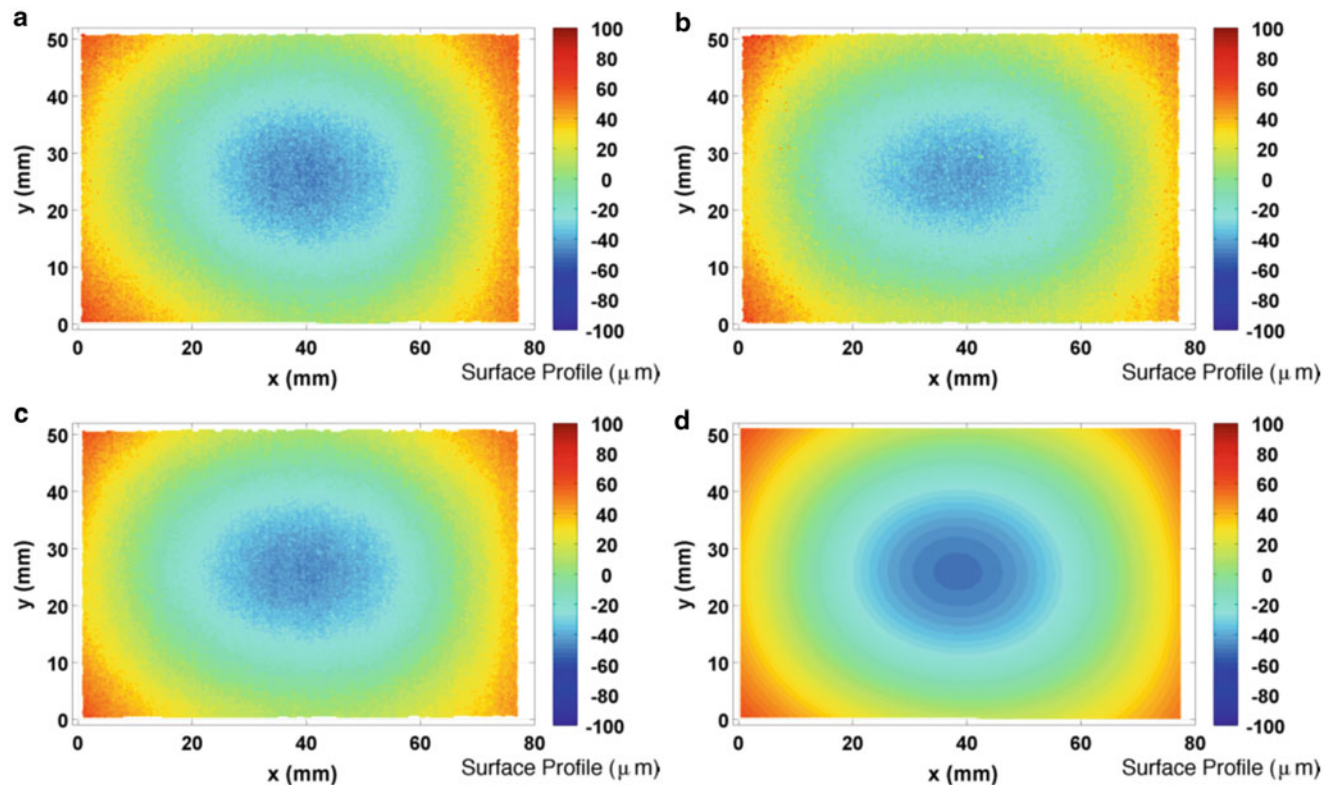


Fig. 40.3 Measured surface displacement from the contour method measurement. (a) Surface “1”, (b) surface “2”, (c) averaged surface, and (d) fitted surface

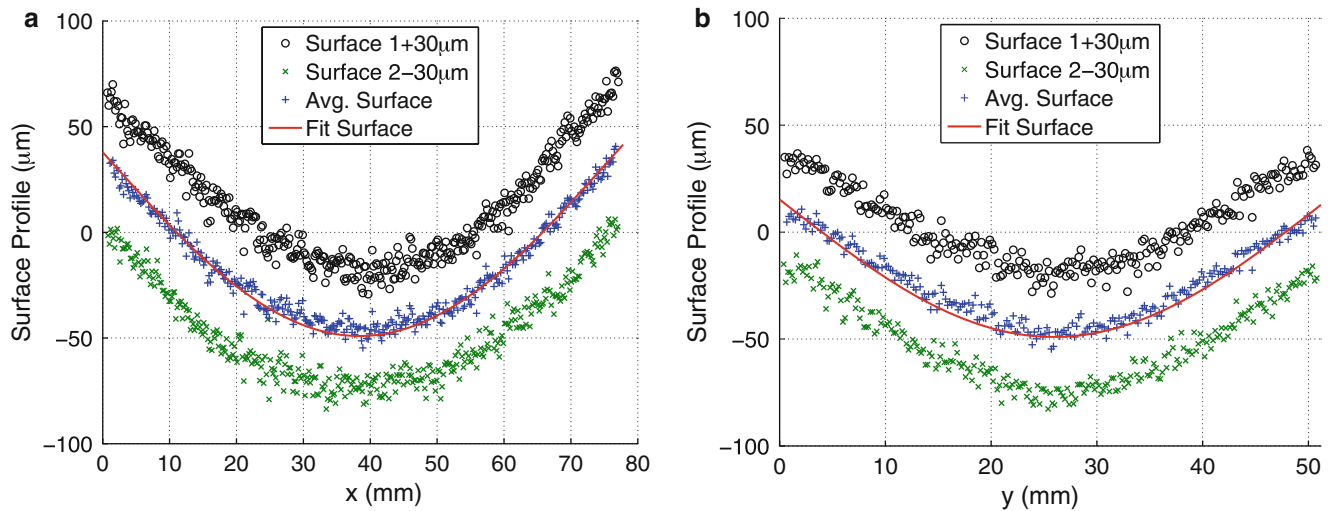


Fig. 40.4 Measured surface displacements along the (a) horizontal direction at mid-vertical dimension and (b) vertical direction at mid-horizontal dimension. Note: the data from surface 1 is offset by 30 μm and the data from surface 2 is offset by -30 μm, so that the average and fit are also visible on the same plot

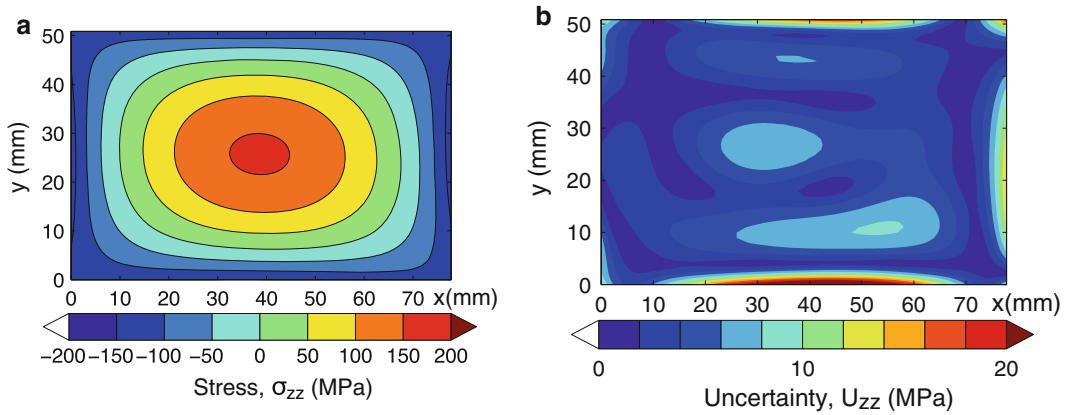


Fig. 40.5 Measured longitudinal (a) stress and (b) uncertainty (68 % confidence interval)

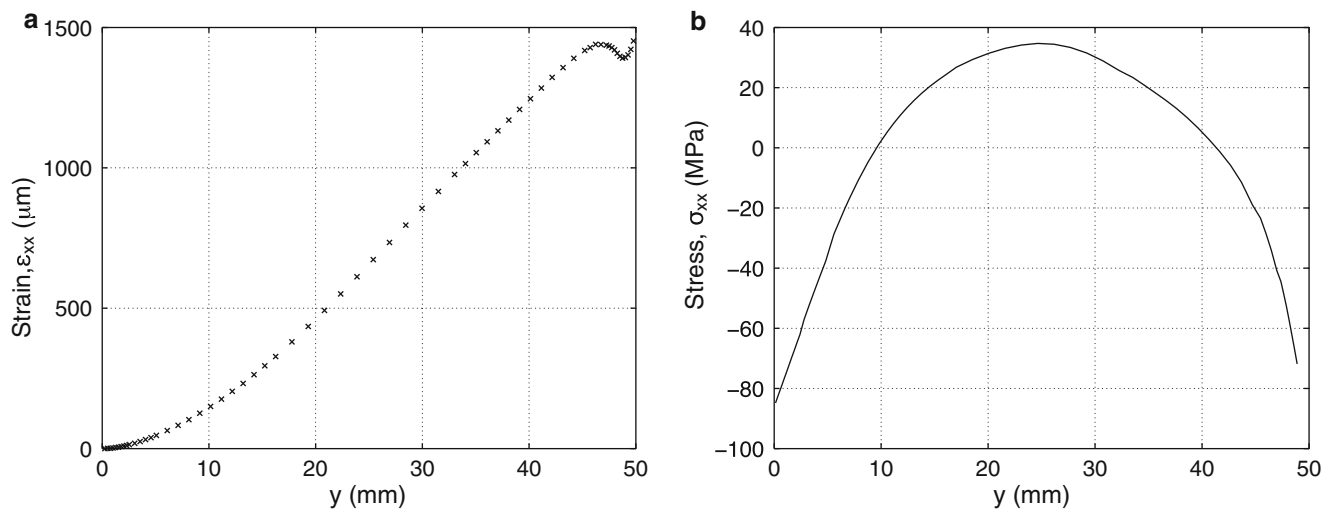


Fig. 40.6 (a) Measured strain and (b) calculated stress for the slitting measurement at x = 18.9 mm

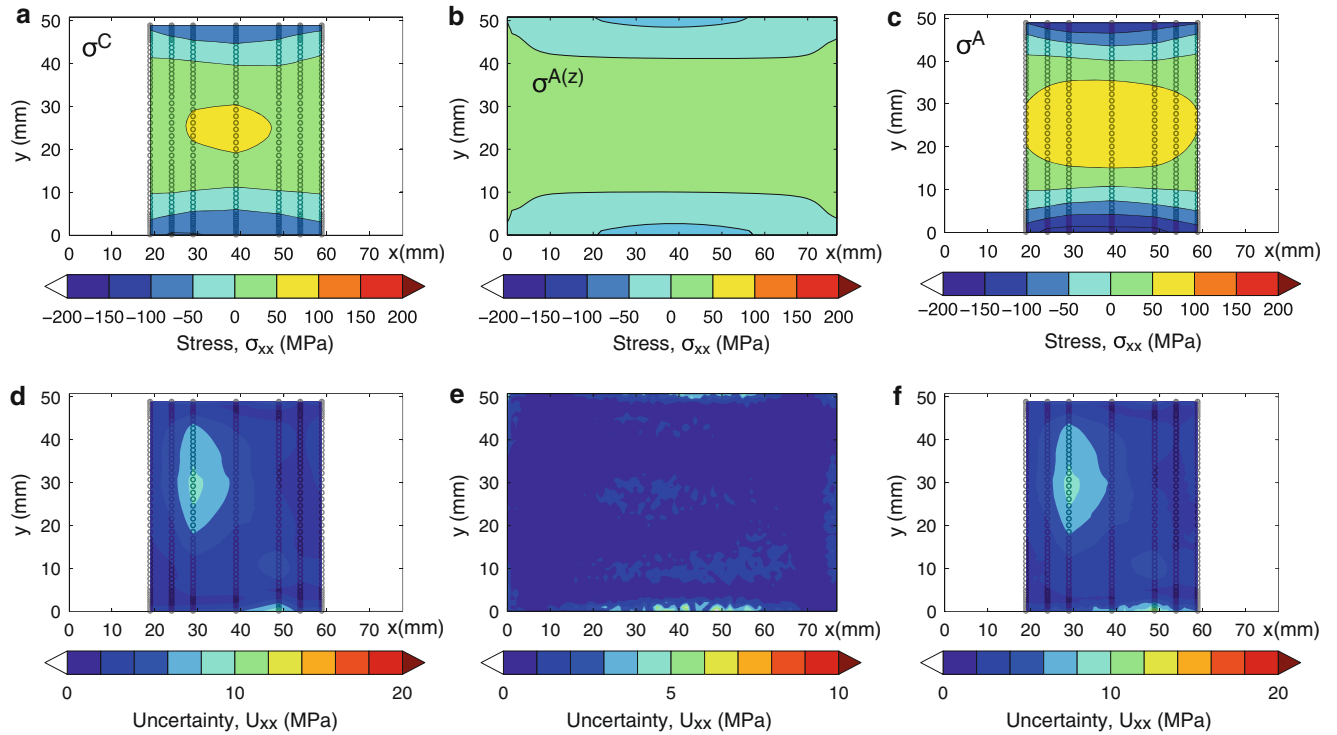
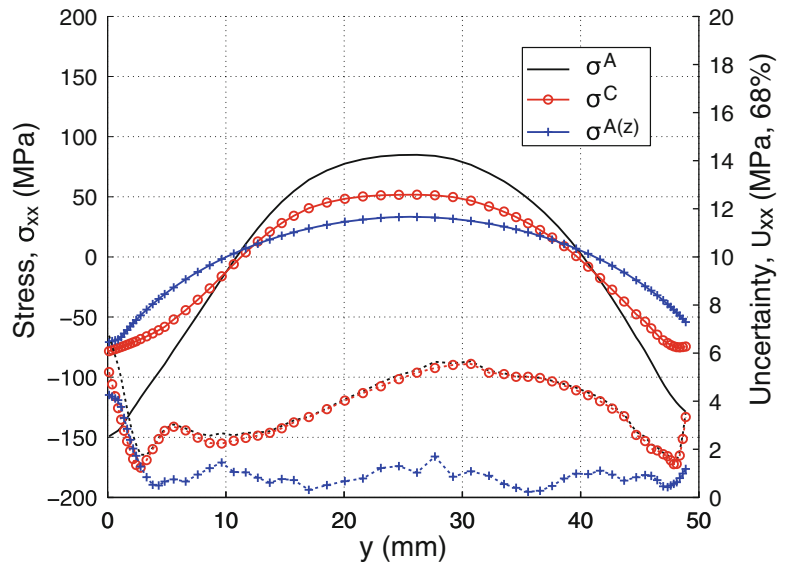


Fig. 40.7 Long transverse stress: (a) remaining in slice, (b) effect of longitudinal stress on the thin slice, and (c) total, with (d–f) showing corresponding uncertainty, at a 68 % confidence interval

Fig. 40.8 Stress and uncertainty of the two contributions to the transverse stress measurement and the total (σ^A), at a horizontal position of 38.9 mm. Uncertainty is shown as *dotted lines* and is further described in [36]



40.3.2 Confirmation Measurements

The results of the three confirmation measurements can be seen in Fig. 40.9. The fitting parameters for the contour measurement at $x=38.9$ mm ($x=x_m$), 19.45 mm ($x=x_m-19.45$), and 58.35 ($x=x_m+19.45$) have $(m, n)=(2, 1)$, $(3, 1)$, and $(3, 1)$, respectively. The results of the confirmation measurement at $x=38.9$ mm shows a roughly parabolic distribution through thickness (away from the edges), with compressive stresses along the exterior (minimum of -160 MPa) and tensile stresses toward the center (maximum of 75 MPa). Results of the other two confirmation measurements, at $x=x_m \pm 19.45$, are

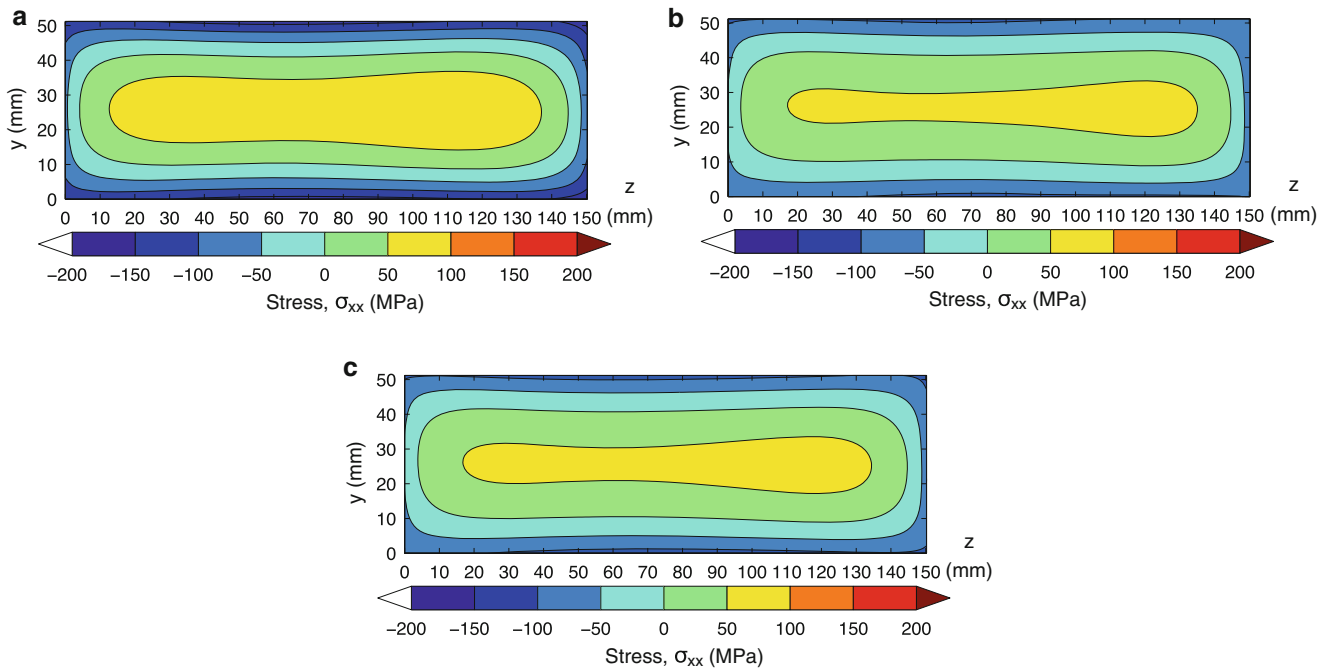


Fig. 40.9 Measured transverse stress at (a) $x=38.9$ mm, (b) $x=18.9$ mm, and (c) $x=58.9$ mm

also parabolic and are self-similar, with lower magnitude than found at $x=38.9$ mm. These features are consistent with a quench stress field.

The transverse stress σ_{xx} from the biaxial map and from the confirmation measurements are compared in Fig. 40.10. Results from two sets of measurements are in agreement at all locations. The largest difference occurs at $x=38.9$ mm, being 25 MPa near $y=50$ mm. However, at most points, the measurements agree well. Overall, the good agreement between the two methods validates the biaxial mapping approach.

40.4 Discussion

The new biaxial mapping method has some advantages over other established residual stress measurement techniques. For example, biaxial mapping measurements in welded components have been shown to be especially useful [20, 33, 34]. In welds, the primary advantage derives from the use of mechanical stress release, which is largely unaffected by the microstructural issues commonly present in welds that very often complicate diffraction based measurements. Furthermore, the use of slitting brings the excellent precision offered by that technique, as compared to somewhat poorer precision of other methods that could be used for mapping stress in the thin slice [35].

One point of concern in developing the biaxial mapping approach is that the superposition of multiple measurements could result in poor precision. However, we have found that not to be the case, as is further discussed in [36]. The uncertainty found in that work shows the transverse stress uncertainty (of the biaxial map) is low, under 10 MPa, in large part because slitting has excellent precision [37, 38]. To contrast, the longitudinal stress, which consisted of a single contour measurement, had somewhat larger uncertainties, up to 20 MPa. The 20 MPa uncertainty found in the contour measurement will affect the uncertainty in $\sigma_{xx}^{A(z)}$, but to smaller degree because the effect of the longitudinal stress on the axial stress in the thin slice is always smaller than the longitudinal stress itself. The uncertainty found here compares favorably with uncertainties typical of other residual stress measurement techniques [39].

Another issue that is relevant for biaxial mapping is the optimal selection of slitting measurement locations. If measurements in the slice are too close to one another, the precision of the measurement decreases. A recent study has addressed this topic [31] and found the minimum distance between slitting planes for good measurement precision is 0.2 times the part thickness.

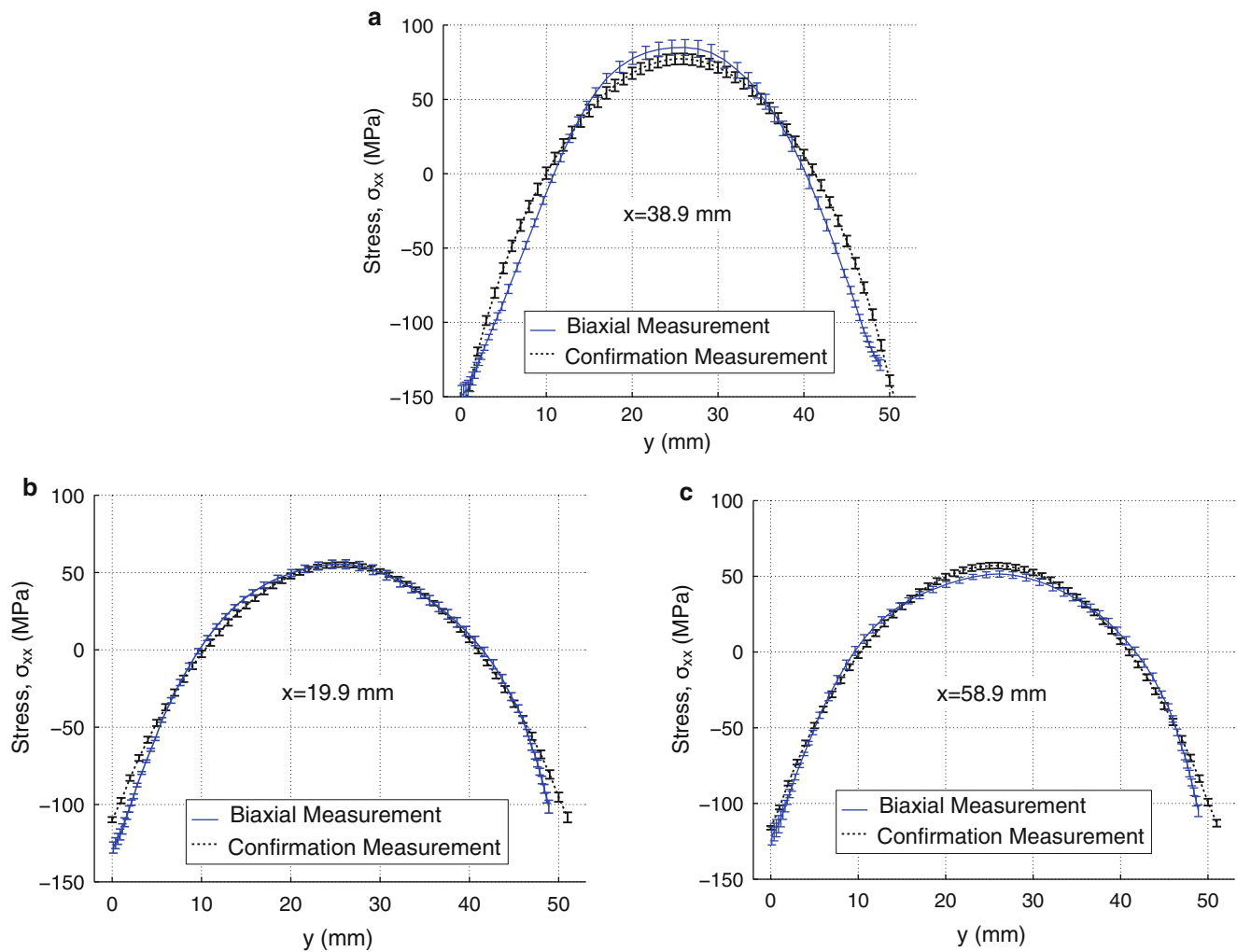


Fig. 40.10 Line plots comparing the biaxial measurement of the transverse stress and the confirmation measurement at x positions (a) 38.9 mm, (b) 19.9 mm, and (c) 58.9 mm

40.5 Summary

A biaxial residual stress mapping approach using mechanical stress release methods was described. The measurement consists of decomposing the initial residual stress into the stress remaining in a thin slice and the effect of the longitudinal stress on that slice. The longitudinal stress is found using the contour method. The effect of the longitudinal stress on a thin slice is found using a finite element computation. The transverse stress remaining in the slice is found using several slitting measurements.

Physical experiments were performed to find a biaxial map of longitudinal and transverse stress in a quenched aluminum bar. Both the longitudinal and transverse stresses were found to have a paraboloid distribution, with tensile stress in the center of the cross-section and compressive stress along the edges, which agrees with the residual stress field typical of quenching. The minimum and maximum of the longitudinal stresses are -153 and 157 MPa and of the transverse stress are -160 and 90 MPa.

The results of the biaxial mapping measurement were compared to confirmation measurements of the transverse stress at three planes. The good agreement with the confirmation measurements validates the biaxial mapping approach.

Acknowledgements The authors acknowledge financial support from the Electric Power Research Institute, Materials Reliability Program (Paul Crooker, Principal Technical Leader). The authors acknowledge helpful discussions with Adrian T. DeWald of Hill Engineering, LLC and Michael B. Prime of Los Alamos National Laboratory.

References

1. M.N. James, D.J. Hughes, Z. Chen, H. Lombard, D.G. Hattingh, D. Asquith et al., Residual stresses and fatigue performance. *Eng. Fail. Anal.* **14**, 384–395 (2007)
2. H. Luong, M.R. Hill, The effects of laser peening on high-cycle fatigue in 7085-T7651 aluminum alloy. *Mater. Sci. Eng. A* **477**, 208–216 (2008)
3. M. Mochizuki, Control of welding residual stress for ensuring integrity against fatigue and stress–corrosion cracking. *Nucl. Eng. Des.* **237**, 107–123 (2007)
4. R. Parrott, H. Pitts, Chloride stress corrosion cracking in austenitic stainless steel, Research Report RR902, Health and Safety Laboratory, 2011
5. J.I. Tani, M. Mayuzumi, T. Arai, N. Hara, Stress corrosion cracking growth rates of candidate canister materials for spent nuclear fuel storage in chloride-containing atmosphere. *Mater. Trans.* **48**, 1431–1437 (2007)
6. EPRI, Material reliability program crack growth rates for evaluating primary water stress corrosion cracking (PWSCC) of alloy 82, 182, and 132 Welds, MRP-115NP, Electric Power Research Institute, 2004
7. P.J. Withers, Residual stress and its role in failure. *Rep. Prog. Phys.* **70**, 2211–2264 (2007)
8. S.H. Bush, Failure mechanisms in nuclear power plant piping systems. *J. Press. Vessel Technol.* **114**, 389–395 (1992)
9. J. Mullins, J. Gunnars, *Validation of Weld Residual Stress Modeling in the NRC International Round Robin Study* (Swedish Radiation Safety Authority, Stockholm, 2013)
10. O. Muránsky, M.C. Smith, P.J. Bendeich, T.M. Holden, V. Luzin, R.V. Martins et al., Comprehensive numerical analysis of a three-pass bead-in-slot weld and its critical validation using neutron and synchrotron diffraction residual stress measurements. *Int. J. Solids Struct.* **49**, 1045–1062 (2012)
11. H.J. Rathbun, L.F. Fredette, P.M. Scott, A.A. Csontos, D.L. Rudland, NRC welding residual stress validation program international round robin program and findings, in *PVP2011-57642, 2011 ASME Pressure Vessels and Piping Division Conference*, Baltimore, MD, USA, 2011
12. EPRI, *Materials Reliability Program: Finite-Element Model Validation for Dissimilar Metal Butt-Welds (MRP-316)* (Electric Power Research Institute, Palo Alto, 2011)
13. H. Ou, J. Lan, C. Armstrong, M. Price, An FE simulation and optimisation approach for the forging of aeroengine components. *J. Mater. Process. Technol.* **151**, 208–216 (2004)
14. L. Zhang, X. Feng, Z. Li, C. Liu, FEM simulation and experimental study on the quenching residual stress of aluminum alloy 2024. *Proc. Inst. Mech. Eng. B J. Eng. Manuf.* **227**, 954–964 (2013)
15. M.T. Hutchings, P.J. Withers, T.M. Holden, T. Lorentzen, *Introduction to the Characterization of Residual Stress by Neutron Diffraction (Chapter 6)* (CRC Press, Boca Raton, 2005)
16. ASTM, *E837, Standard Test Method for Determining Residual Stresses by the Hole-Drilling Strain-Gage Method* (ASTM International, West Conshohocken, 2009)
17. M.B. Prime, Plasticity effects in incremental slitting measurement of residual stresses. *Eng. Fract. Mech.* **77**, 1552–1566 (2010)
18. A. Mahmoudi, S. Hossain, C. Truman, D. Smith, M. Pavier, A new procedure to measure near yield residual stresses using the deep hole drilling technique. *Exp. Mech.* **49**, 595–604 (2009)
19. P. Pagliaro, M.B. Prime, J.S. Robinson, B. Clausen, H. Swenson, M. Steinzig et al., Measuring inaccessible residual stresses using multiple methods and superposition. *Exp. Mech.* **51**, 1123–1134 (2010)
20. M.R. Hill, M.D. Olson, Biaxial residual stress mapping in a PWR dissimilar metal weld, in *PVP2013-97246, ASME 2013 Pressure Vessels and Piping Division Conference*, Paris, France, 2013
21. M.R. Hill, M.D. Olson, A.T. DeWald, Biaxial residual stress mapping for a dissimilar metal welded nozzle, in *PVP2014-28328, ASME 2014 Pressure Vessels and Piping Division Conference*, Anaheim, CA, USA, 2014
22. SAE Aerospace, Heat treatment of wrought aluminum alloy parts, AMS 2770, 2006
23. M.B. Prime, A.T. DeWald, *Practical Residual Stress Measurement Methods (Chapter 5)* (Wiley, West Sussex, 2013)
24. M.R. Hill, *Practical Residual Stress Measurement Methods (Chapter 4)* (Wiley, West Sussex, 2013)
25. M.B. Prime, Cross-sectional mapping of residual stresses by measuring the surface contour after a cut. *J. Eng. Mater. Technol.* **123**, 162–168 (2001)
26. E.M. Shaw, P.P. Lynn, Areal rainfall evaluation using two surface fitting techniques. *Hydrol. Sci. Bull.* **17**, 419–433 (1972)
27. M.B. Prime, Residual stress measurement by successive extension of a slot: the crack compliance method. *Appl. Mech. Rev.* **52**, 75–96 (1999)
28. G.S. Schajer, M.B. Prime, Use of inverse solutions for residual stress measurement. *J. Eng. Mater. Technol.* **128**, 375–382 (2006)
29. M.J. Lee, M.R. Hill, Effect of strain gage length when determining residual stress by slitting. *J. Eng. Mater. Technol.* **129**, 143–150 (2007)
30. C.C. Aydiner, M.B. Prime, Three-dimensional constraint effects on the slitting method for measuring residual stress. *J. Eng. Mater. Technol.* **135**(3), 031006 (2013)
31. M.D. Olson, M.R. Hill, Residual stress mapping with slitting. *Exp. Mech.* (2014 manuscript in preparation for publication)
32. J.S. Robinson, D.A. Tanner, C.E. Truman, A.M. Paradowska, R.C. Wimporoy, The influence of quench sensitivity on residual stresses in the aluminium alloys 7010 and 7075. *Mater. Charact.* **65**, 73–85 (2012)
33. M.D. Olson, M.R. Hill, V.I. Patel, O. Muránsky, T. Sisneros, Measured biaxial residual stress maps in a stainless steel weld. *J. Nucl. Eng. Radiat. Sci.* (2015 accepted for publication)
34. M.D. Olson, M.R. Hill, B. Clausen, M. Steinzig, T.M. Holden, Residual stress measurements in dissimilar weld metal. *Exp. Mech.* **55**(6), 1093–1103 (2015)
35. A.T. DeWald, M.R. Hill, Repeatability of incremental hole drilling and slitting method residual stress measurements. *Residual Stress Thermomech. Infrared Imag. Hybrid Tech. Inverse Probl.* **8**, 113–118 (2014)
36. M.D. Olson, M.R. Hill, A new mechanical method for biaxial residual stress mapping. *Exp. Mech.* **55**, 1139–1150 (2015)
37. M.J. Lee, M.R. Hill, Intralaboratory repeatability of residual stress determined by the slitting method. *Exp. Mech.* **47**, 745–752 (2007)
38. M.B. Prime, M.R. Hill, Uncertainty, model error, and order selection for series-expanded, residual-stress inverse solutions. *J. Eng. Mater. Technol.* **128**, 175 (2006)
39. M.R. Hill, M.D. Olson, Repeatability of the contour method for residual stress measurement. *Exp. Mech.* **54**, 1269–1277 (2014)